Published in final edited form as:

ACS Nano. 2019 October 22; 13(10): 11144–11152. doi:10.1021/acsnano.9b03937.

Subcellular Control Over Focal Adhesion Anisotropy, Independent of Cell Morphology, Dictates Stem Cell Fate

Maria D. Cabezas[†,‡,#], **Brian Meckes**[†,‡,#], **Chad A. Mirkin**[†,‡,§,*], **Milan Mrksich**[†,‡,§,*]

[†]Department of Chemistry, Evanston, Illinois 60208, United States.

[‡]International Institute for Nanotechnology, Evanston, Illinois 60208, United States.

[§]Department of Biomedical Engineering Northwestern University, Evanston, Illinois 60208, United States.

Abstract

Although microscale patterning techniques have been used to control cell morphology and shape, they provide only indirect control over the formation of the subcellular cytoskeletal elements that determine contractility. This paper addresses the hypotheses that nanoscale anisotropic features of patterned matrix can direct the alignment of internal cytoskeletal actin fibers within a confined shape with an unbiased aspect ratio, and that this enhanced control over cytoskeletal architecture directs programmed cell behaviors. Here, large area polymer pen lithography is used to pattern substrates with nanoscale extracellular matrix protein features and to identify cues that can be used to direct cytoskeletal organization in human mesenchymal stem cells. This nanopatterning approach is used to identify how anisotropic focal adhesions around the periphery of symmetric patterns yield an organized and contractile actin cytoskeleton. This work reports the important finding that anisotropic cues that increase cell contractility within a circular shape redirect cell differentiation from an adipogenic to an osteogenic fate. Together, these experiments introduce a programmable approach for using sub-cellular spatial cues to control cell behavior within defined geometries.

Graphical Abstract

[*]**Corresponding authors:** chadnano@northwestern.edu, milan.mrksich@northwestern.edu.

[#]M.D.C. and B.M. contributed equally. M.D.C., B.M., C.A.M., and M.M. conceived experiments, interpreted results, and wrote the manuscript. M.D.C. and B.M. performed experiments.

Financial Interest Statement

The authors declare no competing financial interests

Supporting Information

The supporting information is available free of charge on the ACS Publications website.

The supporting information includes information about quantitative methods used to determine fiber orientation and perform color deconvolution, in addition to a general scheme outlining steps to pattern substrates, images showing hMSCs cultured on distinct square and circular patterns, and immunofluorescence images of cells stained for RUNX2, myosin IIa and vinculin.

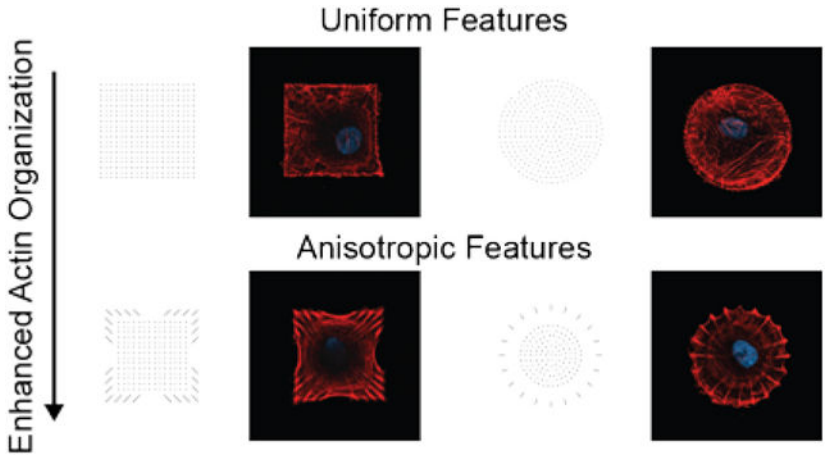

Keywords

cell adhesion; nanopatterning; polymer pen lithography; image analysis; cytoskeleton; actin

The organization of the extracellular matrix (ECM) at both nano and micro length scales directs the formation of focal adhesion (FA) complexes in adherent cells and in turn influences cytoskeletal organization, cell shape, and specific cellular responses such as migration, survival, and differentiation.[1–3] The development of methods that can pattern protein ligands to solid substrates has been important to control cell adhesion[4–13] and to understand the many ways in which cells respond to ECM organization at a range of length scales.[4, 14–20] Importantly, the use of approaches to pattern adhesive cues has provided significant insight into more complex behaviors including migration,[21, 22] differentiation,[23–27] survival,[25, 28, 29] and signaling.[13, 30, 31] Significant work has used microcontact printing to demonstrate how global cell shape directs the formation of focal adhesions at local regions of the cell perimeter.[31–33] It is also commonly observed that FAs adopt an elongated morphology at edges of the cell, with an alignment that corresponds with that of the associated actin stress filaments. Aligned and elongated focal adhesions are also observed in cells cultured on unpatterned substrates, where cell spreading is not restricted to a predefined geometry. This observation raises the question of whether ECM ligands that are patterned into subcellular asymmetric features can in turn direct the organization of the cytoskeleton, with downstream effects on cell behaviors.

A series of landmark studies have demonstrated how substrates that are nanopatterned with ECM ligands can control cell adhesion and influence cell activities. Spatz and coworkers, for example, used micelle block-copolymer lithography to show that a maximal distance of~50–70 nm between individual integrin molecules can still support integrin clustering for effective cell adhesion and spreading, and where greater inter-ligand spacing decreases cell function.[5] Furthermore, nanostructured topographies presenting cell adhesion ligands can enhance osteogenic differentiation when moderate disorder is present, which supports the formation of stable focal adhesions.[34, 35] Other studies further reveal the exquisite sensing capability of cells to respond to nanoscale variations in the size, spacing, composition and topology of patterned cues presented on substrates.[3–6, 8, 30, 36, 37]

While previous studies have explored the influence of cellular-scale anisotropic patterns on cytoskeleton organization and cell behaviors,[12, 22, 38–41] this work addresses the role of anisotropic nanoscale features on cytoskeletal organization within defined geometries (*i.e.* squares and circles). Studies have been limited in exploring the role of feature anisotropy in directing cell behavior, in large part because the patterning methods to control geometry at a sub-micron length scale have not been readily available. Indeed, most high-resolution nanopatterning techniques are labor intensive, time consuming, and provide limited throughput. Here, we use the emerging high throughput, high resolution, large area nanopatterning technique, polymer pen lithography (PPL)[42–45] to pattern sub-micron fibronectin features with aspect ratios of 4–6:1 and we show that the orientation of the fibronectin feature can direct the alignment of the actin stress filaments in adherent cells.[18, 42, 43, 46, 47] PPL can be used to define subcellular protein features in arbitrary size and shape over cm^2 areas, allowing one to probe many cells at once under near-identical conditions, thereby providing a route to statistically meaningful data. Here, we use this technique to nanopattern fibronectin into pre-defined geometries and the subcellular arrangements to test the influence of anisotropy as a cue that directs the assembly of the cytoskeleton and downstream signaling. Significantly, we show that anisotropic focal adhesions provide control over the uniformity and directionality of the actin cytoskeleton. While it has been shown that the anisotropy of focal adhesions increases with increasing cell aspect ratios,[48] our use of PPL allows independent control over cell shape and anisotropic presentation of fibronectin and therefore can provide an understanding of how sub-cellular cues can independently direct assembly of the cytoskeleton with control over contractility and differentiation. Here, we show how this approach has identified two shape factors that enhance osteogenesis.

Results and Discussion

Generating Arbitrary Patterns for Cell Adhesion and Differentiation Studies Using PPL

We used polymer pen lithography (PPL) to rapidly prepare substrates having nanoscale patterns of fibronectin with defined geometries. Pen arrays consisting of ~10,000 polymeric tips were inked with 16-mercaptohexadecanoic acid (MHA) and loaded into a PPL instrument. Patterns of MHA features were generated on gold-coated glass slides (Figure S1a). To validate that patterns were printed successfully, a portion of the gold-coated glass substrates was chemically etched, and the resulting MHA printed substrates were visualized with optical microscopy (Figure S1b). Next, the MHA patterned slides were treated with an ethanolic solution containing a hexa(ethylene glycol)-terminated alkanethiol, which backfilled the unmodified regions of gold with a chemically inert monolayer[18] and which prevents the non-specific protein adsorption in these experiments. Fibronectin was then introduced on the surfaces to allow it to adsorb to the MHA features (Figure S1a). Fluorescence micrographs confirm the discrete localization of antibody-labeled fibronectin on the surface in an arrangement defined by the MHA features (Figure S1c). This process was used to prepare a range of substrates having several arrangements of fibronectin features for subsequent studies of cytoskeletal organization in adherent cells.

Cell Cytoskeleton Organization on Square Geometries

In a first example, we printed an array of square features (54 × 54 μm^2), each consisting of a dot matrix of 19 × 19 square fibronectin features of approximately 750 nm dimension (Figure 1a, e). We cultured human mesenchymal stem cells (hMSCs) on a substrate that presents a uniform distribution of isotropic fibronectin features within the square geometry and which serves as a benchmark for identifying the influence of anisotropic fibronectin features. After 16 hr of culture, we fixed and stained the actin cytoskeleton with a phalloidin-conjugated fluorophore and then imaged the hMSCs using confocal microscopy. We generated heatmaps by superimposing fluorescence micrographs of the actin cytoskeleton; these heatmaps confirmed that the square dot matrix pattern indeed does not induce any directional assembly of actin filaments (Figure 1e, right panel). The distribution of stress fibers, however, localizes along the periphery of the patterned square shape in most hMSCs.

Next, we prepared substrates that were patterned with asymmetric features, to ask whether the orientation and aspect ratio of anisotropic features could control the cytoskeleton, while maintaining constant cell size and shape. Specifically, we asked whether the direction of actin stress filaments would correspond to the orientation of the anisotropic focal adhesions. Hence, we designed and printed a set of patterns having: 1) a center region presenting features arranged in a uniform square dot matrix that would provide sufficient ECM to support cell attachment and 2) a region along the periphery of the pattern where ligand arrangement and aspect ratio are varied (Figures 1b–d). Importantly, the overall shape of the pattern and feature density were approximately identical for the square patterns, and therefore the cells attached to these patterns still maintained a 1:1 aspect ratio.

Fluorescence micrographs of actin fibers reveal that the anisotropic fibronectin features along the perimeter of the square shape could reinforce the alignment of actin fibers when they were aligned with the diagonal axes of the overall shape (Figure 1b). For cells seeded on the inverse anisotropic square patterns where the fibronectin features are oriented perpendicular to the diagonal axis of the cell, actin fibers still preferentially aligned diagonally across the cell (Figure 1c). In contrast, features arranged vertically around the periphery did not induce actin fibers to arrange along the edges of the pattern (Figure 1d). Instead, these cues disrupted the organization of the cytoskeleton observed in the parent pattern.

These results suggest that the cues associated with a square cell shape dominate over those associated with the nanoscale fibronectin features; the corners of square shapes, for example, have been shown to be sites for recruitment of focal adhesions and associated stress filaments. We find that cells on all three patterns having different orientations of the anisotropic fibronectin features share a similar organization of the cytoskeleton that is determined by the global cell shape and not the orientation of the anisotropic fibronectin features. Although, we do find that the pattern having anisotropic fibronectin features aligned with the diagonal axis shows the most organized cytoskeleton (Figure 1b).

To quantitatively assess the role of anisotropic fibronectin feature orientation on actin organization, we performed an in-depth analysis on these cells (Figure 1f). For this analysis,

we compared the distribution of actin fibers in hMSCs on the square dot matrix pattern to those on the anisotropic square of the same size (Figure 1e, f). Heatmaps of the average actin fluorescence intensity show preferential alignment of fibers toward the interior of the cell on the square anisotropic pattern (Figure 1f, right panel). When we quantified fiber orientation using a gradient detection method,[49] the fiber alignment indeed increased along the long axes (+45° and −45°) for cells on anisotropic patterns compared to the square dot matrix (Figure 1g). These results show that the anisotropic arrangement of adhesion ligands supports the assembly of user-directed actin architectures. In addition, when we increased the area of this pattern —where the center region of the dot matrix pattern was increased from 30 × 30 to 40 × 40 μm^2, we found that the anisotropic features had the same influence on cytoskeletal alignment (Figure S2).

MSC Cytoskeleton Organization on Circular Geometries

As described above, the strong global cues of the square patterns—which lead to stress filaments aligned along the diagonals of the cell—dominated over the anisotropic fibronectin features. Hence, we next repeated these experiments using circular patterns, which have been demonstrated to only weakly direct the assembly of the cytoskeleton.[23] In this way, we could determine whether the anisotropic features, absent global shape cues, could direct cytoskeletal assembly. We prepared patterns having a radius of 31 μm because they would have the same area as the square patterns described above. Again, we generated a set of patterns to examine parameters that may affect actin fiber alignment (Figure S3a–h). Previous studies have shown that circumferential and chordal fibers are the primary actin orientations within cells seeded on microcontact printed circular geometries.[50] Therefore, we varied the distribution of fibronectin in two ways: 1) concentric rings were introduced within the circle and 2) periodic, anisotropic features consisting of anisotropic dot lines were placed around the periphery. In addition, all patterns contained a central region presenting fibronectin features arranged in a circular dot matrix that supports cell attachment and spreading.

Fluorescence micrographs confirmed the formation of circumferential and radial actin fibers within hMSCs on all the circular shapes (Figure S3a–h). However, circular shapes with concentric rings of fibronectin features did not significantly change the circumferential fiber distribution within the cells (Figure S3b, d–f). On the other hand, when we introduced anisotropic features radially around the circle, actin fibers assembled in a periodic fashion reflecting the pattern design (Figure S3g). We also note that a sparse spacing between peripheral features promotes different cell geometries that no longer reflect a circular shape (Figure S3h). From this library, we identified a periodic pattern consisting of 20 anisotropic features arranged around the cell periphery that promoted the formation of distinct radial fibers (Figure 2b, c).

We compared cells seeded on the 20-point circle to those seeded on patterns presenting symmetric features arranged in a circular shape (Figure 2a, b). Heatmaps of the average actin intensity reveal a periodicity in the radial fiber distribution within cells on 20-point circles that is not observed when cells are seeded on dot matrix circles (Figure 2c). In order to assess the periodicity of the fibers, the local fiber orientation was determined, and the

fibers were classified as either radial or circumferential depending on the local orientation of the fiber relative to the centroid of the cell (Figure S4). The angular distribution of the radial fibers has a clear periodicity within cells on the 20-point circular pattern (Figure 2d). Fast Fourier transform (FFT) analysis of the fiber distribution confirms an 18° periodicity for the 20-point circles (Figure 2e). In contrast, no periodicity was measured within cells on a dot matrix pattern (Figure 2e).

To determine whether the radial fiber periodicity observed in the cells seeded on the 20-point circle results from cells responding to feature anisotropy or geometric spacing, we generated a hybrid structure that combined the anisotropy of the 20-point circle with the circle dot matrix circle (Figure 2a). After staining for actin, we still observed the formation of strikingly periodic fibers (Figure 2b) and confirmed their periodicity by measuring the angular distribution (Figure 2d). Notably, the periodicity of the actin fibers in cells seeded on the hybrid pattern was weaker than the 20-point circle likely due presence of neighboring features that facilitate redistribution of the actin cytoskeleton. However, this periodicity was significantly higher than the dot matrix circle (Figure 2e). This result demonstrates that the cells have preferential sensing of the anisotropic features even in the presence of a more continuous ECM.

Focal Adhesion Distribution on Patterned Surfaces in Response to Anisotropy

Since focal adhesion complexes link the actin cytoskeleton to the ECM, we examined their distribution within cells seeded on anisotropic, periodic, and dot matrix patterns. Immunofluorescence micrographs of vinculin, a focal adhesion protein, show that the focal adhesions primarily form along the periphery of the cell in locations defined by the underlying pattern (Figure 3a–e). Significantly, the focal adhesion geometry reflects the shape of the underlying pattern, and more importantly, the orientation of the actin stress filament is aligned with the fibronectin feature. These results highlight that the geometry and distribution of adhesive cues lead to focal adhesion formation at desired locations with programmed anisotropy, which directs the actin cytoskeletal architecture.

Modulating hMSC Fate in Response to Focal Adhesion-Defined Actin Arrangements

With the demonstration that anisotropic fibronectin features can direct focal adhesion formation and actin orientation, we investigated whether focal adhesion anisotropy could be used to modulate differentiation independent of cell shape. To evaluate lineage-specific differentiation, we cultured hMSCs on patterns having either anisotropic (anisotropic squares and 20-point circles) or isotropic (square dot matrix and circle dot matrix) ligand arrangements in mixed osteogenic and adipogenic induction media. After 6 days, we fixed and stained cells for osteogenic and adipogenic markers. Cells that stained purple due to alkaline phosphatase activity were counted as osteoblasts while those that stained red from oil droplets (Oil Red O) were counted as adipocytes (Figures 4a, 5a). We also stained the cells with the nuclear dye DAPI and did not score cells that occupied a pattern with a second cell. Color deconvolution was performed on images of single cells to separate and binarize the purple and red channels (Figure S5). The average pixel intensity of each channel was calculated and used to determine if cells were osteogenic or adipogenic (Figures 4b, 5b). Cells with purple channel intensities greater than 2.5 and red channel intensities less than

1.25 were counted as osteogenic, while cells with red channel intensities greater than 1.25 and purple channel intensities less than 2.5 were scored as adipogenic (Figures 4b, 5b). During these experiments approximately one-half the cell population differentiated into osteogenic or adipogenic fates (Figure S6).

Cells grown on both square patterns—the square dot matrix and anisotropic—showed a strong preference for osteogenesis over adipogenesis when cultured on larger patterns (54 × 54 μm^2; Figure 4b–c), as was expected for the strong cue that corners present to a cell and the pro-osteogenic effect of greater spread area.[23, 27] To determine whether focal adhesion anisotropy could synergistically enhance differentiation, we decreased the overall pattern area to reduce the osteogenic cue (36 × 36 μm^2; Figure 4b–c), and we found a stronger preference for osteogenesis for cells seeded on the anisotropic square patterns compared to those grown on the square dot matrix patterns (Figure 4b–c). These results illustrate how anisotropic arrangements of ligands can synergize with global cell shape to promote an osteogenic fate.

Next, we repeated this experiment for cells cultured on circular patterns. These shapes lack any corners along their perimeter and are known to limit the organization of a contractile cytoskeleton, leading to adipogenic fates.[27] As expected, we observed a preference for adipogenesis for cells grown on dot matrix circles (Figure 5b–c). In contrast, cells grown on the 20-point circle patterns preferentially differentiated into osteogenic fates (Figure 5b–c). Significantly, even when cells are grown on the hybrid circle, there is still a preference for osteogenic differentiation. For all of our substrates, cells give mixed populations of the two cell fates, and therefore are not as selective as earlier reports that used mechanical stiffness,[51] cell size,[27] and cell shape.[23] We expect that future work will demonstrate that the anisotropic sub-cellular features we show here can be combined with other parameters to synergistically increase yields for the desired cell type. In addition, we examined the nuclear translocation of RUNX2, a primary regulator of osteogenesis, in cells seeded on the circle patterns by examining the nuclear/cytoplasmic staining intensity. As we found with the alkaline phosphatase stain, cells seeded on the 20-point and hybrid circles showed greater nuclear staining intensity compared to cells seeded on the dot matrix circles (Figure S7). Together, these results demonstrate that the anisotropic fibronectin features, while maintaining a constant shape and size, can redirect cells from primarily adipogenic to osteogenic fates.

Previous work by us and others suggested that the enhanced osteogenesis results from increased contractility of the acto-myosin cytoskeleton in the cell.[23, 27, 52, 53] Therefore, we examined how the anisotropic arrangement of ligands affected the formation of contractile actomyosin fibers (Figure S8). In order to evaluate the actomyosin contractility of hMSCs, we cultured these cells on the square, anisotropic square, circular, and 20-point circle patterns. After 16 hr of culture, cells were fixed and then stained for vinculin, focal adhesions, and myosin IIa. Fluorescent micrographs reveal that myosin IIa is localized along the fibers that have been directed by the anisotropic focal adhesions, suggesting that these user-defined fibers are indeed contractile (for both the square anisotropic and 20-point circle patterns). This observation is especially important for the circular geometry where the 20-point circle drastically alters the contractility by inducing the formation of contractile radial

fibers not present in the dot matrix circle. To confirm that myosin IIa plays a significant role in our differentiation on the patterned substrates, we treated cells on the anisotropic square and 20-point circle patterns with blebbistatin, an inhibitor of myosin IIa. In both cases, the cells reversed from an osteogenic fate to an adipogenic fate (Figure S9). Together, these results suggest that the propensity for these cells to differentiate to osteogenic lineages stems from enhanced contractility induced by anisotropic ligand arrangement.

Conclusions

This work investigates how anisotropic sub-micron patterns of fibronectin can be used to direct organization of the cytoskeleton. We show that arranging focal adhesions in peripheral areas of cells using nanopatterning enables the controlled reorientation of actin fibers within the interior of cells. The work is also significant because it provides a strategy for modulating actin fiber orientation independently of cell shape allowing one to confine cells on substrates and program their cytoskeleton. Indeed, our demonstration that hMSCs could be patterned in circular shapes but still undergo osteogenesis reveals the importance of these anisotropic features in directing cell function. The use of PPL to define discrete nanofeatures was critical in this work because it gives the ability to tailor focal adhesion formation over large areas in any arbitrary shape to modulate and study cell behavior. Although a single chemical cue was used in this study, multiplexing with PPL is possible, potentially, allowing one to study the importance of multiple cues in combination with controlled morphology and contractility in influencing cellular fate. This approach to cellular engineering will enable the modulation of cell behavior in complex biological environments, such as those containing multiple different cell types. It creates opportunities for directing stem cells down different lineages within the same confined space to mimic tissue organization. This ability to control and direct cytoskeletal formation can be extended beyond stem cell differentiation to study and control other biological systems such as neurite formation and cancer metastasis.

Experimental Methods

Substrate Preparation

Glass slides (1.9 cm × 1.9 cm, 0.5 mm thick, Ted Pella) were sonicated for 30 min, rinsed in ethanol, and dried under a stream of N_2. They were mounted in an electron-beam evaporator (Lesker) and when vacuum reached 2×10^{-7} mTorr, 5 nm of Ti and 35 nm of Au were evaporated. Polymer pen arrays having a pen-to-pen distance of 150 μm were prepared using conventional photolithography techniques according to published methods.[42] Arrays were coated with an ethanolic solution of 10 mM MHA (16-mercaptohexadecanoic) (Sigma) solution for 2 min and dried under N_2. After mounting the Au substrate and pen array on the PPL system (Tera Fab M Series, Tera Print), the chamber humidity was held at 45% for patterning. Patterns were programmed in the software with tip-substrate dwell times of 2s. Feature size and quality were confirmed by sacrificing a portion of the substrate, etching Au in the unpatterned areas with a mixed aqueous solution of 13.3 mM $Fe(NO_3)_3$ and 10 mM thiourea, and observing the results under an optical microscope. The patterned substrates were then immersed in an ethanolic solution of 10 mM 1-mercapto-11-undecyl

hexa(ethylene glycol) (Sigma) solution for 1 h to reduce non-specific protein adsorption. After rinsing with ethanol and drying with N_2, the substrates were exposed to 50 μg/mL of human plasma fibronectin (Millipore) in phosphate buffered saline (PBS) and shaken overnight at 4 °C.

Cell Culture

Human MSCs (Lonza) were cultured at 37 °C with 5% CO_2 in Basal growth medium supplemented with MSC growth supplements (Invitrogen), L-glutamine (Invitrogen), and gentamycin sulfate amphotericin-1 (5 μg/ml; Invitrogen). The cells were used between passage 2 and 3. For chemical induction of differentiation, cells were cultured in mixed media (1:1 osteogenic:adipogenic induction media, PromoCell; 0.5 μg/mL, gentamycin). For myosin IIa inhibition studies, 10 μM of blebbistatin (Stem Cell Technologies) was added to the mixed differentiation media. Approximately 20,000 cells were seeded per substrate. Mycoplasma contamination was monitored using MycoAlertPLUS (Lonza) following the manufacturer's instructions.

Immunofluorescence

hMSCs were cultured on patterned substrates overnight and then fixed in 3.7% paraformaldehyde in PBS for 10 min. After gently rinsing thrice with PBS, cells were permeabilized using 0.3% triton X-100 in PBS for 1 min and blocked with a 0.1% Triton X-100 in PBS solution with 3% of bovine serum albumin for 1 h. For immunofluorescence staining of focal adhesions and actin, primary antibody labeling for vinculin was performed in 1% bovine serum albumin (BSA) in PBS overnight at 4 °C with mouse-anti-vinculin (1:500, Abcam AB18058), followed by secondary antibody labeling using Alexa-Fluor 647 labeled goat anti-mouse (1:250, ThermoFisher A21236) for 1 h at room temperature. Samples were rinsed at least twice with 1× PBS and then actin-labeled using Alexa Fluor 568-labeled phalloidin (ThermoFisher) for 30 min at room temperature. Samples were gently washed three times in PBS and mounted onto glass coverslips using Prolong Gold Antifade reagent with DAPI (ThermoFisher).

For immunofluorescence staining of myosin, samples were incubated in a solution containing an antibody produced in rabbit against non-muscle myosin IIa conjugated to Alexa Fluor 488 (1:750, Abcam AB204675) and 1% BSA in PBS for 1 h at 4°C. Vinculin was stained as described above. For RUNX2 staining, hMSCs were prepared for staining as described above. hMSCs were incubated overnight at 4°C in mouse anti-RUNX2 antibodies conjugated to Alexa Fluor 647 (1:500, Santa Cruz Biotechnology, sc-390351).

Histology

hMSCs were seeded on patterned substrates and cultured for 6 days in presence of mixed (adipogenic and osteogenic) media. Samples were then rinsed twice with PBS and fixed with 3.7% formaldehyde for 10 min. After rinsing twice with PBS, samples were permeabilized with a solution of 60% isopropanol in DI H_2O and stained with Oil Red O (Sigma, 60% isopropanol in DI H_2O) for 30 min at room temperature. Samples were then rinsed once with 60 % isopropanol and then once with PBS and stained for alkaline phosphatase (StemTAG, Cell Biolab, Inc) for 1 h at room temperature. Samples were rinsed twice with

PBS and briefly rinsed in DI H_2O before mounting onto glass coverslips using Prolong Gold Antifade reagent containing DAPI. All substrates were imaged using a DAPI filter set and phase contrast microscopy using a 10× objective (Zeiss LSM 800).

Microscopy Image Analysis

To generate heatmaps, images of fluorescence images of fixed/stained cells were aligned, stacked, averaged and pseudo-colored to represent regions of high- and low-density using ImageJ. The orientation of actin fibers in cell micrographs was analyzed using a custom Matlab script that determines orientation using previous reported gradient analysis methods. Briefly, a pixel variance method was used to determine local fiber orientation and magnitude as previously described.[49] A grayscale threshold, as determined using Otsu's method,[54] was applied to the gradient images. To eliminate imaging derived bias from confocal scanning, randomly selected images were rotated along their axis of symmetry. For square and anisotropic square shaped patterns, fibers were detected within the entire cell as well as those within a region of interest (ROI) that was drawn to exclude fibers around the edge of the cell. Histograms of pixel orientation were generated for each cell after grouping fiber orientations along mirrored axes (*e.g.* −45° and 45°).

For detection of fiber orientation in circular patterns (radial *vs* circumferential), the center of the cell was detected by fitting a circle around the cells (details for this procedure are included within the SI) to identify the centroid. The pixel alignment was determined by comparing the detected pixel orientation to the radial coordinates of that pixel relative to the cell centroid. The fibers were classified as either radial (±30° from the radial coordinate), circumferential (90±30° from the radial coordinate), or indeterminate (fiber not fitting within the first 2 groupings). Fast Fourier transform (FFT) analysis was used to determine the angular periodicity of the fibers within a cell.

Color deconvolution on phase contrast images was performed as previously described[23] using ImageJ (See SI). Briefly, the colors were deconvoluted to purple and red channels based upon visual inspection. An intensity cutoff was applied, and the images were binarized (purple and red) to determine cell fate. Cells containing purple were scored as osteocytes while those were red scored as adipocytes.

Statistical Analysis

All data was analyzed using GraphPad PRISM 5 (GraphPad Software, Inc.). For analysis of fiber orientation, the distribution of orientations was assessed using a two-way ANOVA with Bonferroni *post hoc* analysis. Cell differentiation was assessed using a one-way ANOVA with Tukey HSD *post hoc* analysis. Statistical parameters are as follows: Figure 1g ($F_{interaction}$ = 18.19, F = 67.65); Figure 4c (F = 31.37); Figure 5c (F = 7.322);

Supplementary Material

Refer to Web version on PubMed Central for supplementary material.

ACKNOWLEDGMENTS

Research reported in this publication was supported by the National Cancer Institute of the National Institutes of Health under Award Number U54CA199091. The content is solely the responsibility of the authors and does not necessarily represent the official views of the National Institutes of Health. It was also supported by AFOSR awards FA9550-12-1-0141 and FA9550-16-1-0150. B.Meckes acknowledges support from an Eden and Steven Romick Post-Doctoral Fellowship through the Weizmann Institute of Science.

References

1. Delon I; Brown NH, Integrins and the Actin Cytoskeleton. Curr. Opin. Cell Biol 2007, 19, 43–50. [PubMed: 17184985]
2. Frantz C; Stewart KM; Weaver VM, The Extracellular Matrix at a Glance. J. Cell Sci 2010, 123, 4195–4200. [PubMed: 21123617]
3. Geiger B; Spatz JP; Bershadsky AD, Environmental Sensing through Focal Adhesions. Nat. Rev. Mol. Cell Biol 2009, 10, 21–33. [PubMed: 19197329]
4. Lohmuller T; Aydin D; Schwieder M; Morhard C; Louban I; Pacholski C; Spatz JP, Nanopatterning by Block Copolymer Micelle Nanolithography and Bioinspired Applications. Biointerphases 2011, 6, MR1–12. [PubMed: 21428688]
5. Arnold M; Hirschfeld-Warneken VC; Lohmuller T; Heil P; Blummel J; Cavalcanti-Adam EA; Lopez-Garcia M; Walther P; Kessler H; Geiger B; Spatz JP, Induction of Cell Polarization and Migration by a Gradient of Nanoscale Variations in Adhesive Ligand Spacing. Nano Lett. 2008, 8, 2063–2069. [PubMed: 18558788]
6. Cavalcanti-Adam EA; Aydin D; Hirschfeld-Warneken VC; Spatz JP, Cell Adhesion and Response to Synthetic Nanopatterned Environments by Steering Receptor Clustering and Spatial Location. HFSP J. 2008, 2, 276–285. [PubMed: 19404439]
7. Huang J; Grater SV; Corbellini F; Rinck S; Bock E; Kemkemer R; Kessler H; Ding J; Spatz JP, Impact of Order and Disorder in Rgd Nanopatterns on Cell Adhesion. Nano Lett. 2009, 9, 1111–1116. [PubMed: 19206508]
8. Selhuber-Unkel C; Erdmann T; Lopez-Garcia M; Kessler H; Schwarz US; Spatz JP, Cell Adhesion Strength Is Controlled by Intermolecular Spacing of Adhesion Receptors. Biophys. J 2010, 98, 543–551. [PubMed: 20159150]
9. Vignaud T; Galland R; Tseng Q; Blanchoin L; Colombelli J; Thery M, Reprogramming Cell Shape with Laser Nano-Patterning. J. Cell Sci 2012, 125, 2134–2140. [PubMed: 22357956]
10. Mrksich M; Chen CS; Xia YN; Dike LE; Ingber DE; Whitesides GM, Controlling Cell Attachment on Contoured Surfaces with Self-Assembled Monolayers of Alkanethiolates on Gold. Proc. Natl. Acad. Sci. USA 1996, 93, 10775–10778. [PubMed: 8855256]
11. Chen CS; Mrksich M; Huang S; Whitesides GM; Ingber DE, Micropatterned Surfaces for Control of Cell Shape, Position, and Function. Biotechnol. Progr 1998, 14, 356–363.
12. Thery M; Pepin A; Dressaire E; Chen Y; Bornens M, Cell Distribution of Stress Fibres in Response to the Geometry of the Adhesive Environment. Cell Motil. Cytoskeleton 2006, 63, 341–355. [PubMed: 16550544]
13. Jain N; Iyer KV; Kumar A; Shivashankar GV, Cell Geometric Constraints Induce Modular Gene-Expression Patterns Via Redistribution of Hdac3 Regulated by Actomyosin Contractility. Proc. Natl. Acad. Sci. USA 2013, 110, 11349–11354. [PubMed: 23798429]
14. Mrksich M; Whitesides GM, Using Self-Assembled Monolayers to Understand the Interactions of Man-Made Surfaces with Proteins and Cells. Annu. Rev. Biophys. Biomol. Struct 1996, 25, 55–78. [PubMed: 8800464]
15. Lee KB; Lim JH; Mirkin CA, Protein Nanostructures Formed Via Direct-Write Dip-Pen Nanolithography. J. Am. Chem. Soc 2003, 125, 5588–5589. [PubMed: 12733870]
16. Lim JH; Ginger DS; Lee KB; Heo J; Nam JM; Mirkin CA, Direct-Write Dip-Pen Nanolithography of Proteins on Modified Silicon Oxide Surfaces. Angew. Chem. Int. Ed 2003, 42, 2309–2312.

17. Zheng ZJ; Daniel WL; Giam LR; Huo FW; Senesi AJ; Zheng GF; Mirkin CA, Multiplexed Protein Arrays Enabled by Polymer Pen Lithography: Addressing the Inking Challenge. Angew. Chem. Int. Ed 2009, 48, 7626–7629.
18. Giam LR; Massich MD; Hao L; Shin Wong L; Mader CC; Mirkin CA, Scanning Probe-Enabled Nanocombinatorics Define the Relationship between Fibronectin Feature Size and Stem Cell Fate. Proc. Natl. Acad. Sci. USA 2012, 109, 4377–4382. [PubMed: 22392973]
19. Slater JH; West JL, Fabrication of Multifaceted, Micropatterned Surfaces and Image-Guided Patterning Using Laser Scanning Lithography. Method. Cell Biol 2014, 119, 193–217.
20. Wang X; Li S; Yan C; Liu P; Ding J, Fabrication of Rgd Micro/Nanopattern and Corresponding Study of Stem Cell Differentiation. Nano Lett. 2015, 15, 1457–1467. [PubMed: 25697623]
21. Boujemaa-Paterski R; Galland R; Suarez C; Guerin C; Thery M; Blanchoin L, Directed Actin Assembly and Motility. Methods Enzymol. 2014, 540, 283–300. [PubMed: 24630113]
22. Thery M; Racine V; Piel M; Pepin A; Dimitrov A; Chen Y; Sibarita JB; Bornens M, Anisotropy of Cell Adhesive Microenvironment Governs Cell Internal Organization and Orientation of Polarity. Proc. Natl. Acad. Sci. U. S. A 2006, 103, 19771–19776. [PubMed: 17179050]
23. Kilian KA; Bugarija B; Lahn BT; Mrksich M, Geometric Cues for Directing the Differentiation of Mesenchymal Stem Cells. Proc. Natl. Acad. Sci. USA 2010, 107, 4872–4877. [PubMed: 20194780]
24. Shukla A; Slater JH; Culver JC; Dickinson ME; West JL, Biomimetic Surface Patterning Promotes Mesenchymal Stem Cell Differentiation. ACS Appl. Mater. Inter 2016, 8, 21883–21892.
25. Dike LE; Chen CS; Mrksich M; Tien J; Whitesides GM; Ingber DE, Geometric Control of Switching between Growth, Apoptosis, and Differentiation During Angiogenesis Using Micropatterned Substrates. In Vitro Cell. Dev. Biol. Anim 1999, 35, 441–448. [PubMed: 10501083]
26. von Erlach TC; Bertazzo S; Wozniak MA; Horejs CM; Maynard SA; Attwood S; Robinson BK; Autefage H; Kallepitis C; Hernandez AD; Chen CS; Goldoni S; Stevens MM, Cell-Geometry-Dependent Changes in Plasma Membrane Order Direct Stem Cell Signalling and Fate. Nat. Mater 2018, 17, 237–242. [PubMed: 29434303]
27. McBeath R; Pirone DM; Nelson CM; Bhadriraju K; Chen CS, Cell Shape, Cytoskeletal Tension, and Rhoa Regulate Stem Cell Lineage Commitment. Dev Cell 2004, 6, 483–495. [PubMed: 15068789]
28. Thery M; Racine V; Pepin A; Piel M; Chen Y; Sibarita JB; Bornens M, The Extracellular Matrix Guides the Orientation of the Cell Division Axis. Nat. Cell Biol 2005, 7, 947–953. [PubMed: 16179950]
29. Chen CS; Mrksich M; Huang S; Whitesides GM; Ingber DE, Geometric Control of Cell Life and Death. Science 1997, 276, 1425–1428. [PubMed: 9162012]
30. Spatz JP; Geiger B, Molecular Engineering of Cellular Environments: Cell Adhesion to Nano-Digital Surfaces. Meth. Cell Biol 2007, 83, 89–111.
31. Vignaud T; Galland R; Tseng QZ; Blanchoin L; Colombelli J; Thery M, Reprogramming Cell Shape with Laser Nano-Patterning. J. Cell Sci 2012, 125, 2134–2140. [PubMed: 22357956]
32. Petty RT; Li HW; Maduram JH; Ismagilov R; Mrksich M, Attachment of Cells to Islands Presenting Gradients of Adhesion Ligands. J. Am. Chem. Soc 2007, 129, 8966–8967. [PubMed: 17602634]
33. Thery M, Micropatterning as a Tool to Decipher Cell Morphogenesis and Functions. J. Cell Sci 2010, 123, 4201–4213. [PubMed: 21123618]
34. Huang J; Gräter SV; Corbellini F; Rinck S; Bock E; Kemkemer R; Kessler H; Ding J; Spatz JP, Impact of Order and Disorder in Rgd Nanopatterns on Cell Adhesion. Nano Lett. 2009, 9, 1111–1116. [PubMed: 19206508]
35. Dalby MJ; Gadegaard N; Tare R; Andar A; Riehle MO; Herzyk P; Wilkinson CDW; Oreffo ROC, The Control of Human Mesenchymal Cell Differentiation Using Nanoscale Symmetry and Disorder. Nat. Mater 2007, 6, 997. [PubMed: 17891143]
36. Arnold M; Schwieder M; Blummel J; Cavalcanti-Adam EA; Lopez-Garcia M; Kessler H; Geiger B; Spatz JP, Cell Interactions with Hierarchically Structured Nano-Patterned Adhesive Surfaces. Soft Matter 2009, 5, 72–77. [PubMed: 21686049]

37. McMurray RJ; Gadegaard N; Tsimbouri PM; Burgess KV; McNamara LE; Tare R; Murawski K; Kingham E; Oreffo ROC; Dalby MJ, Nanoscale Surfaces for the Long-Term Maintenance of Mesenchymal Stem Cell Phenotype and Multipotency. Nat. Mater 2011, 10, 637–644. [PubMed: 21765399]
38. Jiang X; Bruzewicz DA; Wong AP; Piel M; Whitesides GM, Directing Cell Migration with Asymmetric Micropatterns. Proc. Natl. Acad. Sci. USA 2005, 102, 975–978. [PubMed: 15653772]
39. Tseng P; Di Carlo D, Substrates with Patterned Extracellular Matrix and Subcellular Stiffness Gradients Reveal Local Biomechanical Responses. Adv. Mater 2014, 26, 1242–1247. [PubMed: 24323894]
40. Xia N; Thodeti CK; Hunt TP; Xu Q; Ho M; Whitesides GM; Westervelt R; Ingber DE, Directional Control of Cell Motility through Focal Adhesion Positioning and Spatial Control of Rac Activation. FASEB J. 2008, 22, 1649–1659. [PubMed: 18180334]
41. James J; Goluch ED; Hu H; Liu C; Mrksich M, Subcellular Curvature at the Perimeter of Micropatterned Cells Influences Lamellipodial Distribution and Cell Polarity. Cell Motil. Cytoskeleton 2008, 65, 841–852. [PubMed: 18677773]
42. Eichelsdoerfer DJ; Liao X; Cabezas MD; Morris W; Radha B; Brown KA; Giam LR; Braunschweig AB; Mirkin CA, Large-Area Molecular Patterning with Polymer Pen Lithography. Nat. Protoc 2013, 8, 2548–2560. [PubMed: 24263094]
43. Huo F; Zheng Z; Zheng G; Giam LR; Zhang H; Mirkin CA, Polymer Pen Lithography. Science 2008, 321, 1658–1660. [PubMed: 18703709]
44. Zheng Z; Daniel WL; Giam LR; Huo F; Senesi AJ; Zheng G; Mirkin CA, Multiplexed Protein Arrays Enabled by Polymer Pen Lithography: Addressing the Inking Challenge. Angew. Chem. Int. Ed 2009, 48, 7626–7629.
45. Wong LS; Karthikeyan CV; Eichelsdoerfer DJ; Micklefield J; Mirkin CA, A Methodology for Preparing Nanostructured Biomolecular Interfaces with High Enzymatic Activity. Nanoscale 2012, 4, 659–666. [PubMed: 22159287]
46. Cabezas MD; Eichelsdoerfer DJ; Brown KA; Mrksich M; Mirkin CA, Combinatorial Screening of Mesenchymal Stem Cell Adhesion and Differentiation Using Polymer Pen Lithography. Meth. Cell Biol 2014, 119, 261–276.
47. Cabezas MD; Mirkin CA; Mrksich M, Nanopatterned Extracellular Matrices Enable Cell-Based Assays with a Mass Spectrometric Readout. Nano Lett. 2017, 17, 1373–1377. [PubMed: 28120616]
48. Ray A; Lee O; Win Z; Edwards RM; Alford PW; Kim DH; Provenzano PP, Anisotropic Forces from Spatially Constrained Focal Adhesions Mediate Contact Guidance Directed Cell Migration. Nat. Commun 2017, 8, 14923. [PubMed: 28401884]
49. Quinn KP; Georgakoudi I, Rapid Quantification of Pixel-Wise Fiber Orientation Data in Micrographs. J. Biomed. Opt 2013, 18, 046003. [PubMed: 23552635]
50. Tee YH; Shemesh T; Thiagarajan V; Hariadi RF; Anderson KL; Page C; Volkmann N; Hanein D; Sivaramakrishnan S; Kozlov MM; Bershadsky AD, Cellular Chirality Arising from the Self-Organization of the Actin Cytoskeleton. Nat. Cell Biol 2015, 17, 445–457. [PubMed: 25799062]
51. Engler AJ; Sen S; Sweeney HL; Discher DE, Matrix Elasticity Directs Stem Cell Lineage Specification. Cell 2006, 126, 677–689. [PubMed: 16923388]
52. Ward DF; Salasznyk RM; Klees RF; Backiel J; Agius P; Bennett K; Boskey A; Plopper GE, Mechanical Strain Enhances Extracellular Matrix-Induced Gene Focusing and Promotes Osteogenic Differentiation of Human Mesenchymal Stem Cells through an Extracellular-Related Kinase-Dependent Pathway. Stem Cells Dev. 2007, 16, 467–479. [PubMed: 17610377]
53. Graziano A; d'Aquino R; Cusella-De Angelis MG; Laino G; Piattelli A; Pacifici M; De Rosa A; Papaccio G, Concave Pit-Containing Scaffold Surfaces Improve Stem Cell-Derived Osteoblast Performance and Lead to Significant Bone Tissue Formation. Plos One 2007, 2, e496. [PubMed: 17551577]
54. Otsu N, A Threshold Selection Method from Gray-Level Histograms. IEEE Trans. Syst. Man Cybern 1979, 9, 62–66.

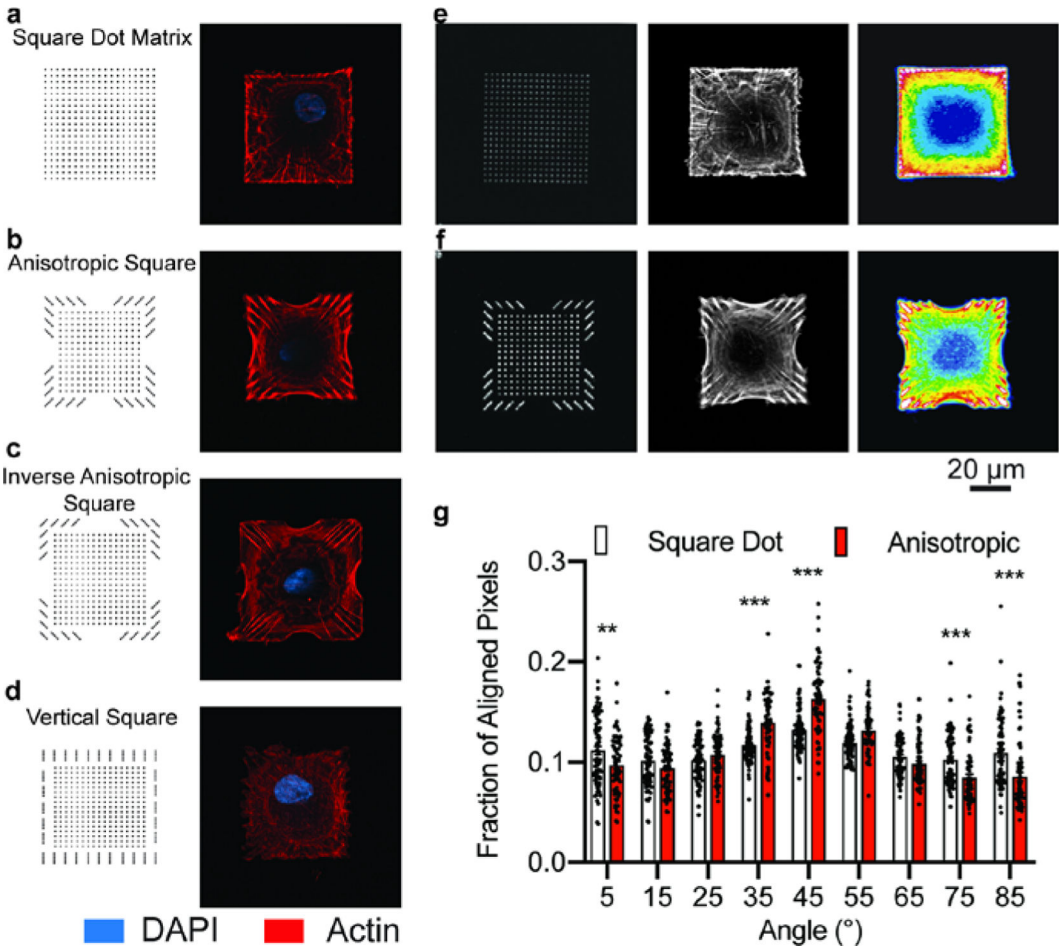

Figure 1. Actin fiber orientation within cells on square substrates.

a-d, Pattern designs (left) and representative fluorescence micrographs of the actin cytoskeleton in hMSCs seeded on each pattern (right). **e**, Fluorescence image of fibronectin patterned as a square dot matrix (left), representative fluorescence image of the actin cytoskeleton of a cell on a square dot matrix pattern (center), heatmap of the average actin fiber staining intensity across population of cells on the square dot matrix substrate (n=78; right). **f**, Fluorescence image of fibronectin patterned as an anisotropic square (left), representative fluorescence image of the actin cytoskeleton of a cell on an anisotropic square pattern (center), heatmap of the average actin fiber staining intensity across populations of cells on the anisotropic square substrate (n=64; right). **g**, The actin fiber orientation within cells on anisotropic and square dot matrix patterns. (mean ± s.e.m.; ** $p<0.01$, *** $p<0.001$, two-way ANOVA with Bonferroni *post hoc*).

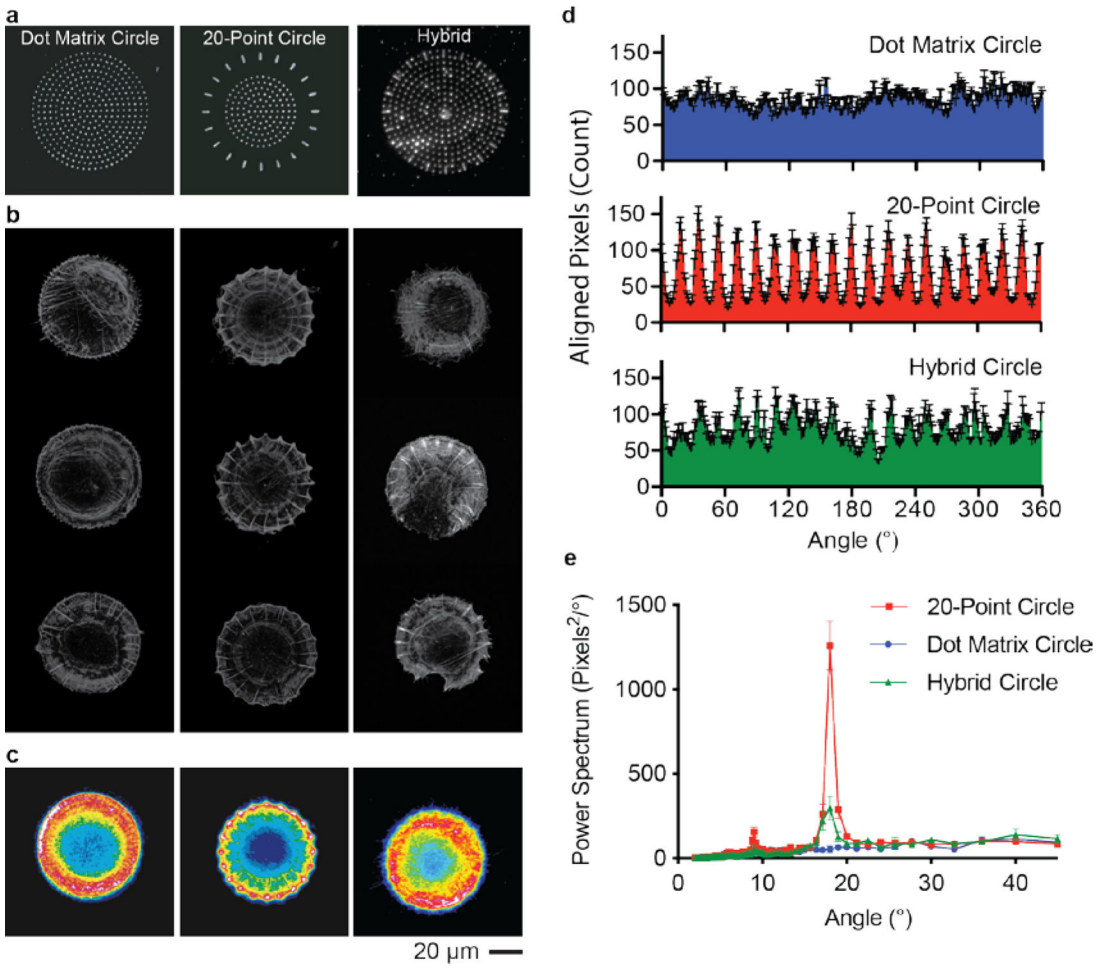

Figure 2. Actin fiber orientation within cells on circular substrate.

a, Fluorescence micrograph of fibronectin patterned in different circular shapes. **b**, Representative fluorescence images of the actin cytoskeleton of cells seeded on each pattern. **c**, Heatmap of the average actin fiber staining intensity across populations of cells on each circle pattern (n=84), 20-point circles (n=57), and hybrid circles (n=46). **d**, The angular distribution of radial fibers within the cells on all three circular patterns (mean ± s.e.m.). **e**, FFT of the angular distribution of the radially oriented actin fibers (mean ± s.d.).

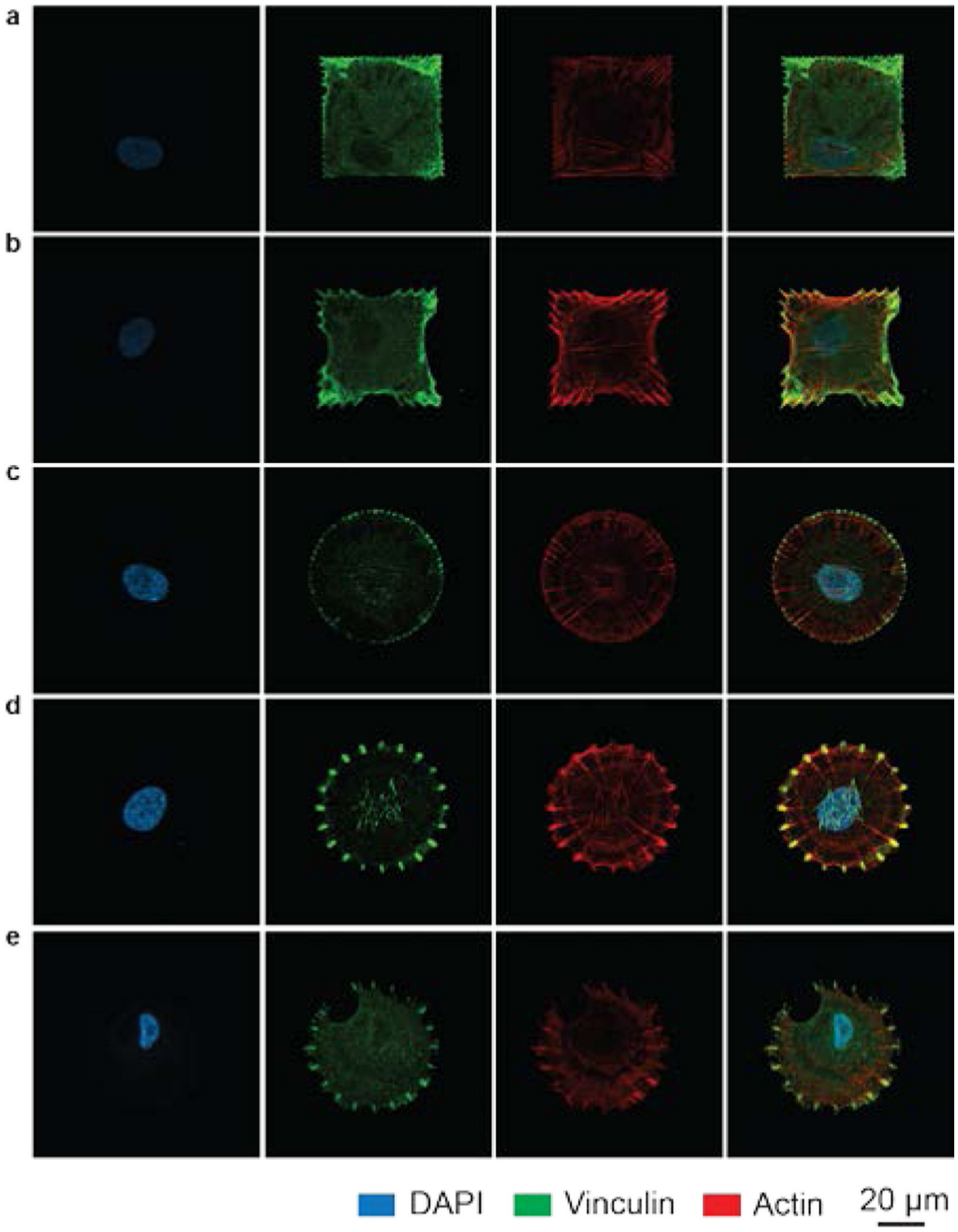

Figure 3. Fluorescence micrographs of the focal adhesions and actin cytoskeleton within cells on patterns.

a-e, Representative confocal images of single cells grown on different patterns: square dot matrix (**a**), anisotropic square (**b**), dot matrix circles (**c**), 20-point circles (**d**), and hybrid circles (**e**). The nucleus (**Panel 1**), focal adhesions (vinculin, **panel 2**), and actin cytoskeleton (**panel 3**) are labeled within each cell. **Panel 4** shows the overlay of the different structures.

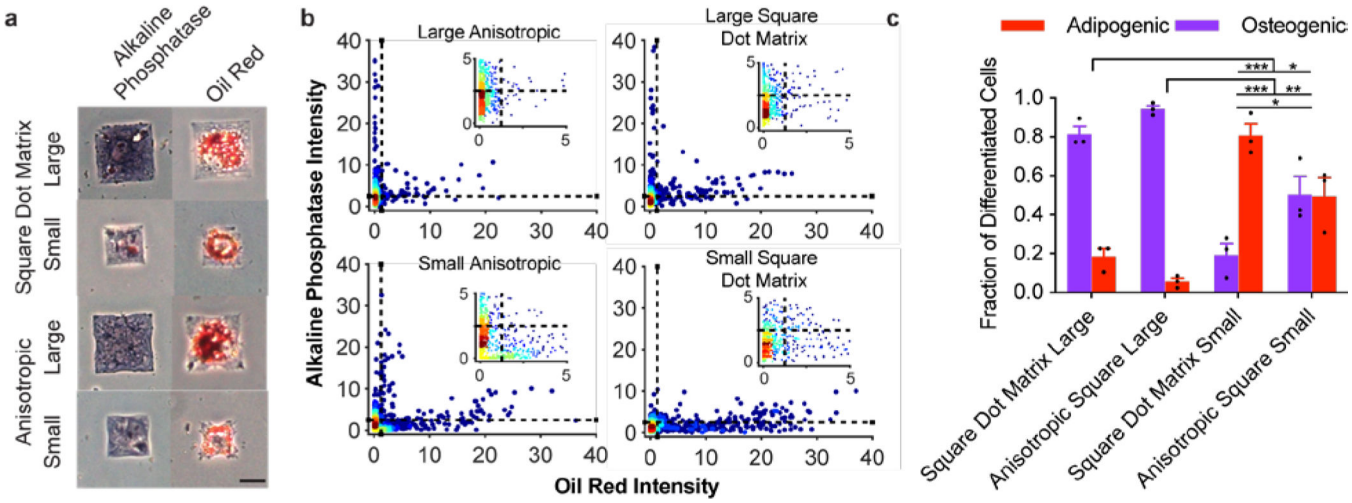

Figure 4. Osteogenic and adipogenic differentiation on square patterns.

a, Brightfield images of cells on each respective pattern strongly staining purple, as an osteogenic marker (left column), or red, as an adipogenic marker (right column). Scale bar: 25 μm. **b**, Scatter plots for staining intensity of individual cells after color deconvolution of the red and purple channels from 3 substrates (ncells = 759–817). **c**, Percentage of cells staining positive for only adipogenic or osteogenic markers (mean ± s.e.m.; *** $p<0.001$; * $p<0.05$; one-way ANOVA with Tukey HSD).

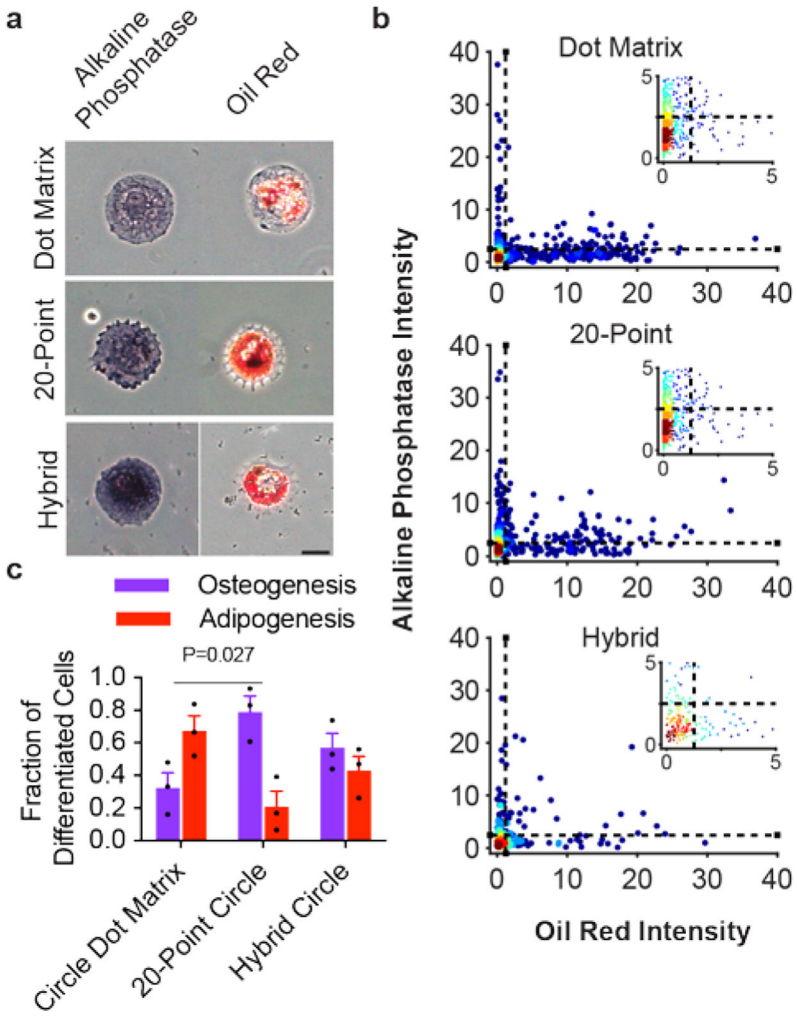

Figure 5. Osteogenic and adipogenic differentiation on circular patterns.

a, Brightfield images of cells on each respective pattern strongly staining purple as an osteogenic marker (left column) or red as an adipogenic marker (right column). Scale bar: 25 μm. **b**, Scatter plots of staining intensity of individual cells after color deconvolution of the red and purple channels from 3 substrates (ncells = 263–849). **c**, Percentage of cells staining positive for only adipogenic or osteogenic markers (mean ± s.e.m.; p=0.027; one-way ANOVA with Tukey HSD *post-hoc*).